Aalborg Universitet

AALBORG UNIVERSITY

User Effects on the Circular Polarization of 5G Mobile Terminal Antennas

Syrytsin, Igor A.; Zhang, Shuai; Pedersen, Gert F.; Ying, Zhinong

Published in:
I E E E Transactions on Antennas and Propagation

DOI (link to publication from Publisher):
10.1109/TAP.2018.2851383

Publication date:
2018

Document Version
Accepted author manuscript, peer reviewed version

Link to publication from Aalborg University

Citation for published version (APA):
Syrytsin, I. A., Zhang, S., Pedersen, G. F., & Ying, Z. (2018). User Effects on the Circular Polarization of 5G Mobile Terminal Antennas. *I E E E Transactions on Antennas and Propagation*, *66*(9), 4906-4911. Article 8399838. https://doi.org/10.1109/TAP.2018.2851383

General rights
Copyright and moral rights for the publications made accessible in the public portal are retained by the authors and/or other copyright owners and it is a condition of accessing publications that users recognise and abide by the legal requirements associated with these rights.

- Users may download and print one copy of any publication from the public portal for the purpose of private study or research.
- You may not further distribute the material or use it for any profit-making activity or commercial gain
- You may freely distribute the URL identifying the publication in the public portal -

Take down policy
If you believe that this document breaches copyright please contact us at vbn@aub.aau.dk providing details, and we will remove access to the work immediately and investigate your claim.

Downloaded from vbn.aau.dk on: May 02, 2026

This article has been accepted for publication in a future issue of this journal, but has not been fully edited. Content may change prior to final publication. Citation information: DOI 10.1109/TAP.2018.2851383, IEEE Transactions on Antennas and Propagation

User Effects on the Circular Polarization of 5G Mobile Terminal Antennas

Igor Syrytsin, Shuai Zhang, Gert Frølund Pedersen, *Member, IEEE*, Zhinong Ying, *Senior Member, IEEE*

***Abstract*—User effects on a circularly polarized phased array for 5G mobile applications for frequencies around 28 GHz are studied in this paper. Two figures of merit are defined: the total scan pattern and coverage efficiency of the circular polarization (CP). The user effects on the performance of a CP phased array are studied via two defined parameters. The investigations are carried out in talk mode (with a hand and a head) and in data mode (with a homogeneous whole-body phantom). The scattering properties of the proposed phantom are verified via the measurement of an antenna with known radiation parameters and a human. The CP coverage efficiency is relatively less affected by biological tissues than by the conventional coverage efficiency, though the absolute value of the CP coverage efficiency depends on a specific design. When user effects are introduced, the axial ratio (AR) bandwidth becomes approximately 0.8 to 1.3 GHz narrower. To realize the optimal CP performance and reduce the user effects of the CP coverage efficiency, a CP array at the bottom short edge of the ground plane should be chosen in talk mode, while the top short edge location should be chosen in data mode.**

***Index Terms*—User effects, circular polarization, phased array, mobile handset antenna, 5G antenna, phantom.**

I. Introduction

THE millimeter/centimeter-wave (mm/cm-wave) frequencies have become an attractive candidate for 5G communication systems where phased arrays should be implemented at both mobile terminals and base stations [1]. Such arrays have been designed to increase the coverage performance of the mobile antenna as in [2] and [3]. Applying a circularly polarized antenna can create multiple benefits when communicating over a wireless medium. In [4], the delay spread can be reduced to 5 ns or even lower if highly directive CP antennas are applied. At 26 GHz, the measurements in [5] have shown that for an indoor non-line of sight (NLOS) scenario, the received signal strength depends on the polarization of the receiving and transmitting antennas. A channel with both Tx and Rx vertical polarization (VP) can be over 10 dB stronger than a channel with both Tx and Rx horizontal polarization (HP). By using a CP or polarization-reconfigurable phased arrays, there can be benefit to keeping the received power at high levels.

Human tissues are well known to be materials with high loss and high permittivity, which will likely affect the performance of mobile terminal antennas. The user impact on mobile terminal antennas has been extensively studied previously for low-frequency bands, such as GSM and LTE in [6] and for cm-waves in [7]. The user effects on the coverage efficiency of mobile phased arrays have been investigated at 3.5 GHz in [8] and at 15 GHz in [9]. A significant loss in the coverage efficiency was observed for both 3.5 GHz and 15 GHz. However, the user effects on the circular polarization (CP) performance of the phased antenna arrays have not been well analyzed at higher frequencies, e.g., between 26 and 31 GHz. In this paper, the user impact on the circular polarization performance of the mobile phased antenna array will be investigated for 5G applications.

This work was supported by the Innovationsfonden project of RANGE.(Corresponding author: Shuai Zhang).

Igor Syrytsin, Shuai Zhang, and Gert Frølund Pedersen are with the Antennas, Propagation and Millimeter-wave Systems section at the Department of Electronic Systems, Aalborg University, Denmark (email: {igs,sz,gfp}@es.aau.dk).

Zhinong Ying is with the Corporate Technology Office, Sony Mobile Communication AB, Lund, Sweden.

A mobile circularly-polarized antenna array with end-fire radiation will be used in this investigation. User effects on the circular polarization performance of the phased antenna array along the frequency range from 26 to 31 GHz will be studied by simulations in CST Microwave Studio transient time domain solver. Two setups with the user will be considered: talk mode, with hand and head, and data mode, with a proposed whole-body homogeneous phantom. Then, the parameters of CP total scan pattern (TSP) and CP coverage efficiency will be introduced to quantify the effects of the user on the CP performance of the array.

II. Geometry and Free-Space Performance

The proposed array element consists of a magnetic dipole and an electric dipole. These two dipoles produce electric fields normal to each other with a 90° phase difference as described in [10]. The antenna is printed on a Rogers 3003 substrate with a thickness of 1.52 mm. The geometry of each antenna element is shown in Fig. 1. The vertical electric field is produced by two identical patches of 4.4 mm × 1.8 mm on each side of the ground plane. The horizontal electric field is produced by the two mirrored dipole arms with the length of 3.7 mm. The antenna is fed between the two patches to obtain a 90° phase difference between the fields, as shown in Fig. 1(a). The patches are connected by two vias with a radius of 0.45 mm. In this paper, the axial ratio (AR) beamwidth and AR bandwidth have been calculated according to the specification of AR $\leq$ 3 dB level. The AR beamwidth and AR bandwidth of the antenna will change with clearance size. Thus, a clearance of 10 mm is selected to obtain a reasonable AR beamwidth and AR bandwidth for this study. The electrically large ground plane of the phone chassis and substrate properties will affect the antenna performance of the low-frequency antenna designs in [10] and [11] at 28 GHz.

Grounding walls and holes were added to the design to suppress the unwanted surface waves. The proposed antenna has a -10 dB and -6 dB impedance bandwidth of 973 MHz (3.475 %) and 2.07 GHz (7.393 %), respectively. The fractional bandwidth was calculated at the central frequency of 28 GHz.

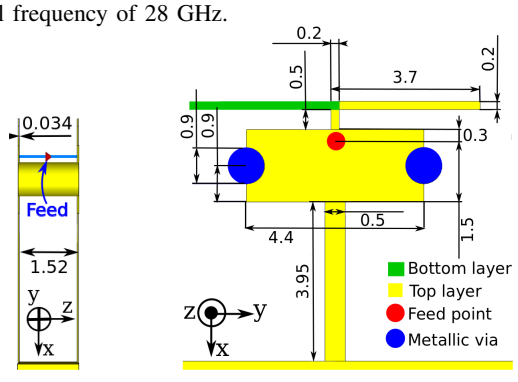

(a) (b)

Fig. 1. Geometry of the antenna element in (a) xz-plane and (b) in xy-plane (Unit: mm).

A. Array Geometry

The proposed phased array is shown in Fig. 2. A total of 8 elements are combined into a linear array on the short edge of the ground

0018-926X (c) 2018 IEEE. Personal use is permitted, but republication/redistribution requires IEEE permission. See http://www.ieee.org/publications_standards/publications/rights/index.html for more information.

This article has been accepted for publication in a future issue of this journal, but has not been fully edited. Content may change prior to final publication. Citation information: DOI 10.1109/TAP.2018.2851383, IEEE Transactions on Antennas and Propagation

plane. The antenna array's main lobe direction and the ϕ scan angle are illustrated in Fig. 2. The distance between elements is 7.6 mm (0.7λ).

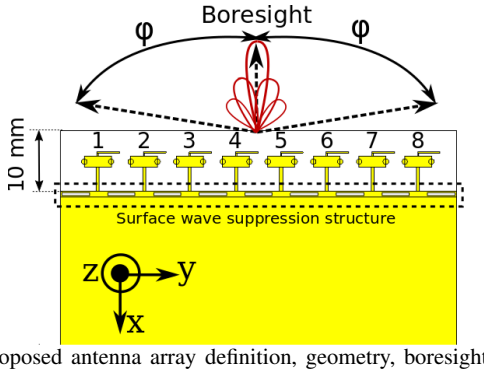

Fig. 2. Proposed antenna array definition, geometry, boresight and scan angle.

B. Free-Space Performance

The maximum gain of the array and the AR at the boresight (with in-phase elements) are shown in Fig. 3(a). The AR bandwidth of 4 GHz can be achieved. Maximum gain over 10 dBi is realized from 26 to 31 GHz.

When a beam is scanned into different directions in ϕ plane, the AR at the main beam direction for each scan angle is shown in Fig. 3(b) at 28 GHz. Please note that the curves in Fig. 3(b), Fig. 11, Fig. 12, Fig. 15 and Fig. 16 are plotted at 28 GHz but that similar tendencies have also been observed at the other frequencies in the band. The AR beamwidth (AR $\leq$ 3 dB) of 55° can be realized by the phased array. The maximum gain within the scanning range is over 11 dBi.

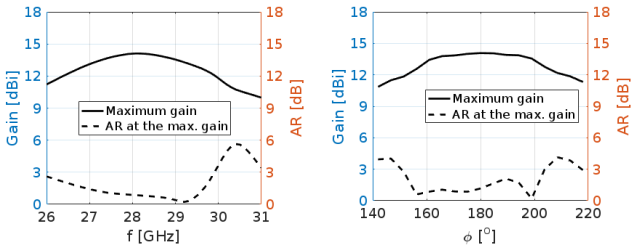

(a) (b)

Fig. 3. Performance of the proposed phased antenna array: (a) maximum gain and AR vs. frequency when the relative phase-shift between antenna elements is 0° and the (b) maximum gain and AR vs scan angle ϕ at 28 GHz.

C. Figure Of Merit

Next, the coverage performance of the array is investigated. The coverage efficiency is calculated from the total scan pattern (TSP) of the phased array, which is shown in Fig. 4(a). The TSP is obtained from all phased array patterns, corresponding to the different scan angles, by recording the best achievable gain at every angular distribution point.

The regular coverage efficiency has been defined as [2]:

$$\eta_c = \frac{\text{Coverage Solid Angle}}{\text{Maximum Solid Angle}} \tag{1}$$

where the maximum solid angle defined as 4π steradians. A CP coverage efficiency specifies the coverage efficiency defined in [2] with respect to the antenna's circular polarization performance. The CP coverage efficiency can be calculated from the total scan pattern by only considering the points in space where AR $\leq$ 3 dB. The CP coverage efficiency is defined in this paper as:

$$\eta_{c,CP} = \frac{\text{Coverage Solid Angle}\big|_{AR<3\,\text{dB}}}{\text{Maximum Solid Angle}} \tag{2}$$

where the maximum solid angle is defined as 4π steradians.

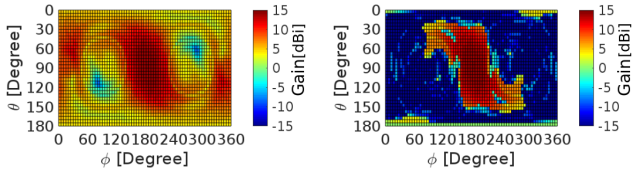

(a) (b)

Fig. 4. (a) Total scan pattern in a general case and (b) CP total scan pattern at 28 GHz.

The regular and CP coverage efficiencies of the array in free space are shown in Fig. 5. For the threshold gain lower than 5 dBi, the CP coverage efficiency of the curve is at least 0.4 lower than the corresponding free-space regular coverage efficiency curve. Moreover, the CP coverage efficiency curve cannot easily reach 100 % of coverage, which is limited by the CP performance of the proposed antenna. The free-space CP coverage curve is at $\eta_c = 0.6$ level for the gain lower than -20 dBi in Fig. 5.

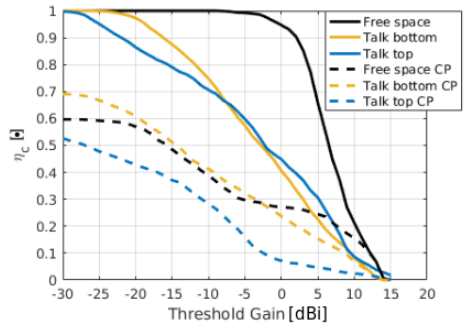

Fig. 5. Comparison of the regular coverage efficiency and CP coverage efficiency between the free space and talk mode.

III. Accuracy Verification of Simulations with Phantom

It is important to notice that CP measurements with the user are very time consuming and challenging. It is difficult to make the user sit/stand still for a prolonged period of measurement. These measurement setup challenges will lead to instability in the phase of the measured pattern. If the measured phase is not correct, then performing the beamforming correctly is nearly impossible. Therefore, simulations with realistic phantoms for data and talk modes have been done in CST Microwave Studio FDTD solver instead of the measurements. Furthermore, at the time of the writing, no standards for human gestures at high frequencies were available.

A. Phantom Description

For the data mode, a phantom is proposed in this paper for 28 GHz, and is shown in Fig. 6(a). The homogeneous full-body phantom is made of skin tissue with the dielectric permittivity of $\varepsilon_r = 16.5 + j16.5$. The parameters of different tissues (including skin) for up to 100 GHz have been measured in [12]. The proposed phantom dimensions are based on the mean values instead of using a specific human specimen. The length of the limbs for the whole-body phantom are chosen according to the average male human dimensions described in [13]. The average weight and body circumference are based on the measurements in [14]. The detailed dimensions of the phantom are shown in Table I. On the other hand, in the talk mode,

0018-926X (c) 2018 IEEE. Personal use is permitted, but republication/redistribution requires IEEE permission. See http://www.ieee.org/publications_standards/publications/rights/index.html for more information.

This article has been accepted for publication in a future issue of this journal, but has not been fully edited. Content may change prior to final publication. Citation information: DOI 10.1109/TAP.2018.2851383, IEEE Transactions on Antennas and Propagation

the hand and head phantom gestures defined in the existing CTIA standards are used [15]. The skin tissue dielectric constant is chosen to be a value similar to that used for the whole-body phantom.

The use of the skin-only phantom is justified because the waves will not penetrate deep into the human tissue at these frequencies. For example, the skin depth at 28 GHz can be calculated as:

$$\delta_s = \sqrt{\frac{\rho}{\pi \cdot f \cdot \mu}} = 4.708\,\text{mm} \tag{3}$$

where ρ is a resistivity of the human tissue chosen to 245 Ωcm or 245E6 μΩcm [16], f is a frequency, and $\mu = \mu_0 \cdot \mu_r$ is skin permeability. For this calculation the $\mu_r = 1$ has been chosen. The phantom can be used to evaluate mobile antenna performance in data mode at a frequency of 28 GHz.

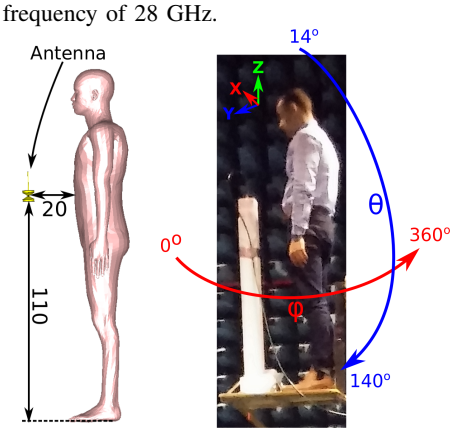

(a) (b)

Fig. 6. Setup with biconical antenna used in (a) simulation and (b) measurement (Unit: cm).

Table I. Dimensions of the phantom and the measured user.

Category	Phantom	User
Height	175.6 cm	174 cm
Neck circumference	42.8 cm	43 cm
Upper arm length	25 cm	24 cm
Upper arm circumference	27.8 cm	32 cm
Lower arm length	27 cm	27.7 cm
Wrist circumference	15 cm	16 cm
Chest circumference	108 cm	111 cm
Waist circumference	89 cm	86 cm
Hip circumference	101 cm	97 cm
Upper leg length	40 cm	40 cm
Lower leg length	50 cm	45 cm
Ankle circumference	22 cm	22 cm

B. Scattering Properties of the Phantom

The phantom's accuracy is verified by measuring the linearly polarized omnidirectional UWB antenna proposed by [17] in two orientations. The chosen antenna has a gain of approximately 5 dBi at 28 GHz. The measurements were made in an anechoic chamber using a single dual-polarized probe antenna in the far field. To remove the uncertainty of the user grip, the antenna is suspended during free-space simulations (Fig. 6(a)) and placed on a foam stand during the measurements (Fig. 6(b)). The coordinate system used in both measurement and simulation is shown in Fig. 6(b).

The measured user has some of the dimensions of the phantom's but different body types. In Table I, the dimensions of the user can be compared to the dimensions of the phantom. In Fig. 7, the simulated and measured radiation patterns with each user and different antenna orientations are shown. In general, the measured and the simulated patterns have a similar shape. The measurements are relatively more noisy due to the cable and connector used for the prototype in the 28 GHz band. In addition, the shadowing sizes are slightly different due to the difficulty of maintaining the exact same antenna position during the measurements. Furthermore, the user's gestures cannot be identical to the simulations.

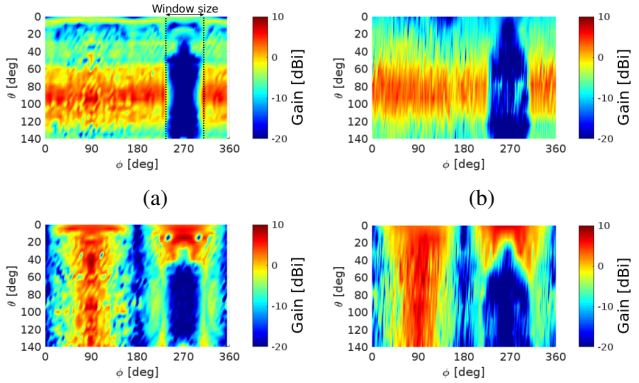

(a) (b) (c) (d)

Fig. 7. Radiation pattern at 28 GHz of (a) simulated antenna - θ polarized, (b) measured antenna - θ polarized, (c) simulated antenna - ϕ polarized, and (d) measured antenna - ϕ polarized.

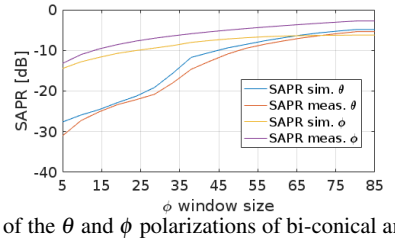

Fig. 8. SAPR of the θ and ϕ polarizations of bi-conical antenna simulated with the phantom and measured with the user.

Next, the shadowing region (around 270° in Fig. 7) in the measured and simulated radiation patterns was investigated. The shadowing antenna power ratio (SAPR) metric is used for this investigation and defined in [7] as:

$$SAPR(\Delta\theta, \Delta\phi) \triangleq \frac{P_{shadow\ in\ the\ window}}{P_{total}} \tag{4}$$

where $\Delta\theta = \theta_{max} - \theta_{min}$ is a window length in θ. Here, 140° is chosen, which is the maximum measured θ range. $\Delta\phi = \phi_{max} - \phi_{min}$ is a variable window, the size of which varies from 1° to 85°. The example of the *phi* window size is marked in Fig. 7(a). The window is centered around ϕ = 270°. P_{shadow} is the power in the shadow (in the chosen area of a radiation pattern). P_{total} is the total radiated power of the antenna.

The formula describes how much lower the power is in the shadow compared to the total radiated power (TRP). In Fig. 8, the SAPR has been calculated for the ϕ and θ polarized radiation patterns of the bi-conical antenna in the measurements and simulations. The SAPR curves for the ϕ and θ polarizations have a very similar tendency in dB. The small difference between the simulated and measured results is because of the same reasons for those in Fig. 7. In general, the proposed phantom has similar external (scattering) properties as the real human user.

From this section, it can be concluded that a proposed phantom can be used to model the scattering properties of the user. This is concluded based on the investigation of the shadowing region created by the user's body and on corresponding calculations of SAPR for the theta and phi polarized antennas.

IV. Talk Mode Simulations

In this section, the phased array described in subsections II-A and II-B have been studied in talk mode, where the user is holding the

0018-926X (c) 2018 IEEE. Personal use is permitted, but republication/redistribution requires IEEE permission. See http://www.ieee.org/publications_standards/publications/rights/index.html for more information.

This article has been accepted for publication in a future issue of this journal, but has not been fully edited. Content may change prior to final publication. Citation information: DOI 10.1109/TAP.2018.2851383, IEEE Transactions on Antennas and Propagation

mobile device close to the ear in the right hand. Investigations were performed to quantify the user effects on regular and CP coverage efficiency, AR bandwidth and AR beamwidth. In the simulation, more than 41 million mesh cells were used. The smallest cell size was 0.05 mm and the largest mesh cell size was 0.856 mm. The setup with the user's head and hand (talk mode) is shown in Fig. 9. The array is located on the bottom of the device in Fig. 9(a) or on the top in Fig. 9(b). The mobile device was placed according to the test standards as defined in [15], and the distance between the ear and the phone chassis was 4 mm.

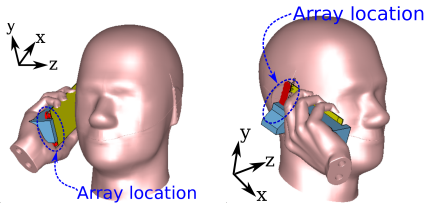

(a) (b)

Fig. 9. User setup with the proposed phased antenna array on the (a) bottom and (b) top.

A. AR Bandwidth

The AR and maximum gain are plotted in Fig. 10(a) for the bottom antenna location. The AR has less than 3 dB from 27 to 30.2 GHz, which corresponds to an AR bandwidth of 3.2 GHz. The AR bandwidth is 0.8 GHz lower than the free-space AR bandwidth. Maximum gain is at least 1 dB lower than in the case of free space. The AR and maximum gain are plotted in Fig. 10(b) for the top antenna location. Heavier shadowing is observed because the array is closer to the user's head. The AR is lower than 3 dB from 27.3 to 30 GHz, which corresponds to the AR bandwidth of 2.7 GHz. The AR bandwidth is 1.3 GHz and 0.5 GHz smaller than the case of the free space and when the antenna is located on the bottom, respectively. Maximum gain is actually 2 dB higher than the maximum gain in the free space due to scattering from the head.

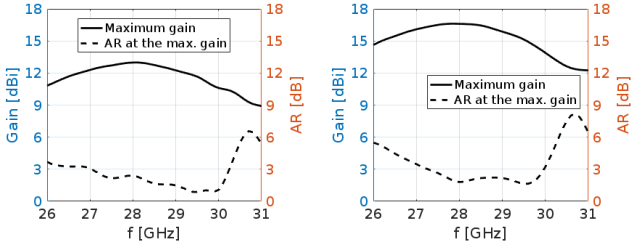

(a) (b)

Fig. 10. Axial ratio and maximum gain vs. frequency for (a) talk mode – bottom antenna location and (b) talk mode – top antenna location when the relative phase shift between antenna elements is 0°.

B. AR Beamwidth

The AR and maximum gain are plotted vs. scan angle in Fig. 11. The AR beamwidth of the array in talk mode – bottom location in Fig. 11(a) is around 55° from ϕ = 155 to 210°. Additionally, the gain for scan angles larger than ±35° (with respect to the boresight (180°)) is over 4 dB lower than that in the free space. The AR and maximum gain for the top antenna location are plotted vs. scan angle in Fig. 11(b). The AR beamwidth is around 40°. The maximum gain in the range from 150 to 190° is 2 dB higher than that in the free space.

C. Total Scan Pattern

Regular and CP TSPs for the array top and bottom locations in the talk mode are shown in Fig. 12. The shadowing area created by

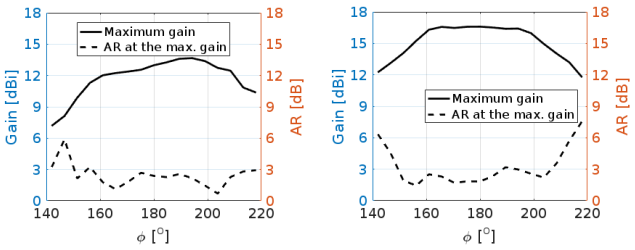

(a) (b)

Fig. 11. Axial ratio and maximum gain at 28 GHz vs. scan angle ϕ for (a) talk mode – bottom antenna location and (b) talk mode – top antenna location.

the user's head and hand appears in all the TSPs. The regular TSP for the bottom antenna location in Fig. 12(a) is weaker than the one produced by the antenna in the free space in Fig. 4(a). However, the CP TSP for the same user setup in Fig. 12(b) is similar to the one in the free space in Fig. 4(b). Thus, the user has relatively less impact on the array CP performance when the bottom location is chosen.

When the array is located on the top edge, the shadowing occurs in the region from $\theta = 0$ to 60°. The regular TSP in Fig. 12(c) is around 2 dB stronger when $\theta = 110°$ and $\phi = 180°$ and has a different shape from the TSP in the free space in Fig. 4(a). Circular polarization only occurs in the small area around $\theta = 100°$ and $\phi = 180°$ in Fig. 12(d).

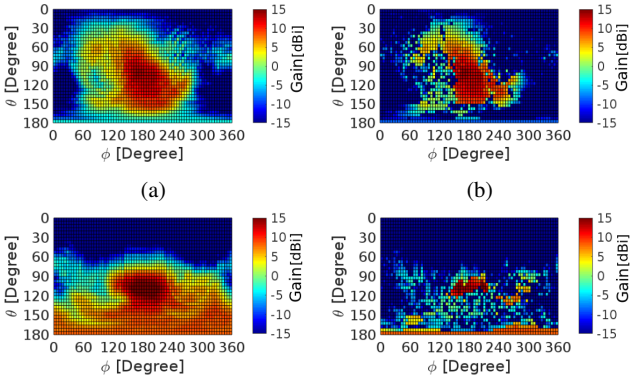

(a) (b) (c) (d)

Fig. 12. Total scan patterns for talk mode at 28 GHz for (a) antenna on bottom – regular TSP, (b) antenna on bottom – CP TSP, (c) antenna on top – regular TSP, and (d) antenna on top – CP TSP.

D. Coverage Efficiency

Regular and CP coverage efficiency curves are shown in Fig. 5. CP coverage efficiency is calculated from the CP total scan pattern using Equation 2. The regular coverage efficiency is calculated using Equation 1. It can be observed that regular coverage efficiency has very similar values for both top and bottom positions. However, the CP coverage efficiency for the threshold gain lower than 8 dBi is 10 to 15 % higher for the bottom position than for the top position.

V. Data Mode Simulations

In this section, the simulations of the phased array are completed in data mode with the whole-body phantom described in Section III. The chosen gestures are shown in Figure 13. In data mode, the user holds the mobile phone in front of the eyes with one hand. The angles used in this phantom setup are in the comfortable zone of a user as described in [13]. The distance between the head and the mobile device is approximately 28 cm. The coordinate system is always similar with respect to the mobile device ground plane to compare the array's total scan patterns simulated with user effects and in the free space. The simulations are performed with CST Microwave

0018-926X (c) 2018 IEEE. Personal use is permitted, but republication/redistribution requires IEEE permission. See http://www.ieee.org/publications_standards/publications/rights/index.html for more information.

This article has been accepted for publication in a future issue of this journal, but has not been fully edited. Content may change prior to final publication. Citation information: DOI 10.1109/TAP.2018.2851383, IEEE Transactions on Antennas and Propagation

Studio with an FDTD solver and over 600 million mesh cells. The smallest cell size is 0.1 mm, and the largest cell size is 1.8 mm. A frequency range from 26 to 31 GHz is used.

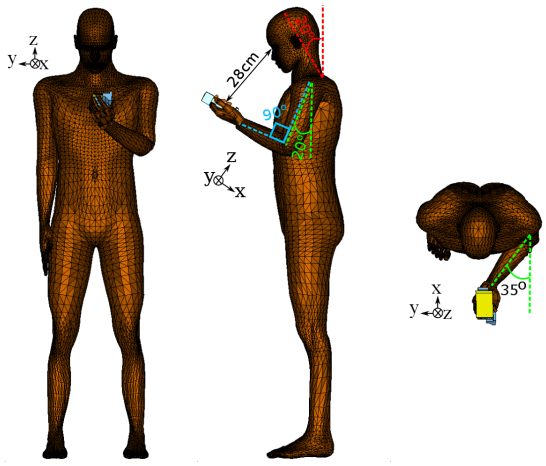

(a) (b) (c)

Fig. 13. Simulation setup in data mode with a homogeneous whole-body phantom shown in (a) front view, (b) side view, and (c) top view.

A. AR Bandwidth

The AR and maximum gain are plotted in Fig. 14 for the bottom and top antenna locations in data mode. For the top antenna location in Fig. 14(a) the AR bandwidth is 3 GHz (10.71 %), which is 1 GHz smaller than that in the free space. Maximum gain on average resembles the free-space case. The AR and maximum gain are plotted in Fig. 14(b) for the bottom antenna location. The AR in the band for the bottom antenna position is worse than 18 dB and, thus, is not visible in the figure. In this case, the array is pointed towards the user, and the main beam is blocked by the user.

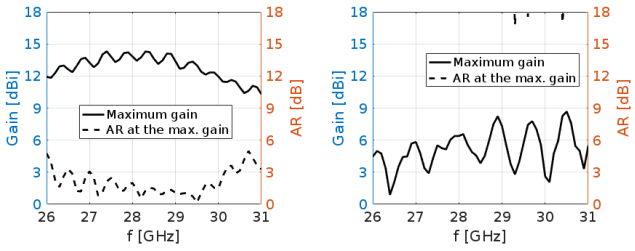

(a) (b)

Fig. 14. Axial ratio and maximum gain vs. frequency for (a) data mode – top antenna location and (b) data mode – bottom antenna location when the relative phase shift between antenna elements is 0°.

B. AR Beamwidth

The AR and maximum gain are plotted vs. scan angle in Fig. 15. For the array top location, the AR beamwidth of 20° is observed in Fig. 15(a). However, the AR is also lower than 3 dB when ϕ = 200° and ϕ = 160°. The maximum gain is comparable to the gain in the free space. The AR and maximum gain in data mode with the bottom location are plotted vs. scan angle in Fig. 15(b).The AR curve can never reach 3 dB and the maximum gain is lower than 0 dBi.

C. Total Scan Pattern

Regular and CP TSPs for the antenna array at the top and bottom locations in data mode are shown in Fig. 16. The regular TSP for the top antenna location is given in Fig. 16(a), which approximates the result in the free-space case shown in Fig. 4(a). The only difference

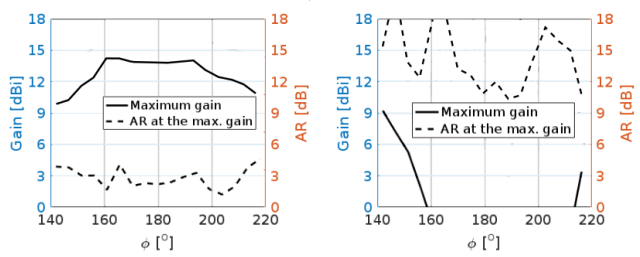

(a) (b)

Fig. 15. Axial ratio and maximum gain vs. ϕ scan angle at 28 GHz for (a) data mode – top antenna location and (b) data mode – bottom antenna location.

is the presence of a shadow at ϕ = 0 and ϕ = 360°. Furthermore, the CP TSP in Fig. 16(b) is nearly identical to the one in the free space in Fig. 4(b). Thus, the user's hand and the body have virtually no impact on the antenna array CP performance when the array is located on the top. The TSP is plotted in Fig. 16(c) and Fig. 16(d) for the bottom antenna location. The shadow from the phantom is extremely strong, and only a small portion of the total is diffracted around the user. Furthermore, CP antenna performance is nonexistent when the antenna is located on the bottom.

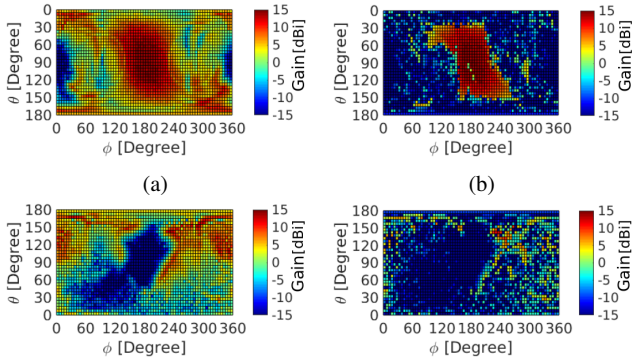

(a) (b)

(c) (d)

Fig. 16. Total scan patterns in data mode at 28 GHz for the (a) antenna array on top – regular TSP, (b) antenna array on top – CP TSP, (c) antenna array on bottom – regular TSP, and (d) antenna array on bottom – CP TSP.

D. Coverage Efficiency

Fig. 17 shows the comparison of the coverage efficiency in data mode and in the free space. The CP curves for the free-space and top antenna locations have similar coverage for the threshold gain from 3 to 9 dBi. The CP coverage of the array in the bottom location is less than 10 % for gain from 0 to 7 dBi. All the curves for the CP coverage efficiency are similar below the threshold gain value of -5 dBi.

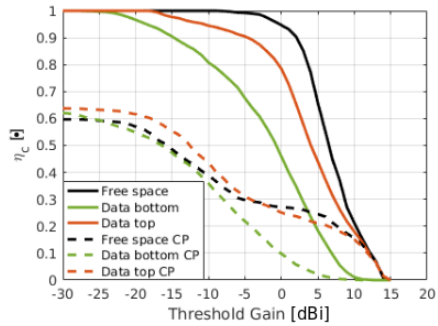

Fig. 17. Comparison of the regular coverage efficiency and CP coverage efficiency between the free space and data mode.

0018-926X (c) 2018 IEEE. Personal use is permitted, but republication/redistribution requires IEEE permission. See http://www.ieee.org/publications_standards/publications/rights/index.html for more information.

This article has been accepted for publication in a future issue of this journal, but has not been fully edited. Content may change prior to final publication. Citation information: DOI 10.1109/TAP.2018.2851383, IEEE Transactions on Antennas and Propagation

VI. Comparison

Comparisons between various simulated antenna parameters are shown in this section. The comparison of the AR bandwidth and AR beamwidth is summarized in Table II. In all cases, a significant loss in AR bandwidth was observed when the array is held by the user. However, AR beamwidths of similar value were achieved in talk mode – bottom location. For the other setups, the AR values are higher than 3 dB and can been observed for the different scan angles because of the user proximity. The CP array cannot be used in the data mode – bottom antenna location because of blockage by the user. In all cases, shadowing is mainly induced by the user's head and body. Furthermore, the user's arm and hand partially contribute to the shadowing. However, in data mode, the shadowing from the head is small in comparison with the body shadowing. On the other hand, in talk mode, the main shadowing source is the user's head.

Table II. AR bandwidth and AR beamwidth and coverage efficiency at 28 GHz for different simulation setups.

Setup	AR bandwidth	AR beamwidth
Free space	4 GHz	55°
Talk mode – top	2.7 MHz	40°
Talk mode – bottom	3.2 GHz	55°
Data mode – top	3 GHz	20°
Data mode –bottom	None	None

The comparison of the coverage efficiency is shown in Fig. 18(a). The solid lines show regular coverage efficiency, and the dashed lines show CP coverage efficiency. As expected, the best regular coverage can be achieved by using the antenna array in the data mode - top location. All other regular coverage efficiency curves have a spread of a minimum of 10 dB. For the threshold gain $\leq$ -5 dBi all of the CP coverage efficiencies have a similar level except for talk mode – top location. For the threshold gain higher than -5 dBi, the curves for the data – top and talk-bottom have very similar coverage. The CP coverage performance of the array in talk-top and data-bottom locations has a similar shape but 5 to 15 % less coverage compared to the data top and talk bottom positions. Furthermore, the CP coverage efficiency curves are 15 to 25 % lower than the free-space curves for the threshold gain lower than 0 dBi. Coverage efficiency curves for the talk bottom and data top positions are plotted in dB in Fig. 18(b) to demonstrate the relative difference between the user and free space cases. In the region ($\leq$ 7 dBi), CP coverage efficiency is relatively less sensitive to user effects.

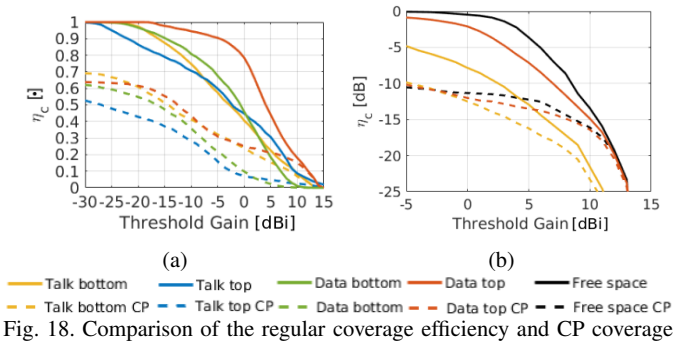

Fig. 18. Comparison of the regular coverage efficiency and CP coverage efficiency for free space, talk mode and data mode plotted (a) in numbers and (b) in dB.

VII. Conclusion

In this paper, user effects on a circular polarized phased array were studied for 5G mobile terminal applications. Two figures of merit have been introduced: the CP total scan pattern and CP coverage efficiency. The user effects on the CP performance of a mobile phased array were studied with the two defined parameters. The CP phased array was studied in talk mode (according to CTIA standards) and in data mode (with the CTIA hand and a homogeneous whole-body phantom). The antenna array was placed at the bottom and top locations on the mobile device ground plane. Circular polarization was relatively more robust to user impact than linear polarization if an array is placed in the right position of the ground plane. To realize the optimal CP performance with user effects in the talk mode, a CP phased array should be placed at the bottom short edge location, while in the data mode, the top short edge location should be used. As a result, the two phased antenna arrays should be placed on the top and bottom edge of the mobile device for optimal antenna performance.

References

[1] T. S. Rappaport, S. Sun, R. Mayzus, H. Zhao, Y. Azar, K. Wang, G. N. Wong, J. K. Schulz, M. Samimi, and F. Gutierrez, "Millimeter wave mobile communications for 5G cellular: it will work!," *IEEE Access*, vol. 1, pp. 335–349, 2013.

[2] J. Helander, K. Zhao, Z. Ying, and D. Sjöberg, "Performance analysis of millimeter-wave phased array antennas in cellular handsets," *IEEE Antenna Wireless Propag. Lett.*, vol. 15, pp. 504–507, 2016.

[3] S. Zhang, X. Chen, I. Syrytsin, and G. F. Pedersen, "A planar switchable 3D-coverage phased array antenna and its user effects for 28 GHz mobile terminal applications," *IEEE Trans. Antennas Propag.*, 2017 (in press).

[4] T. Manabe, Y. Miura, and T. Ihara, "Effects of antenna directivity and polarization on indoor multipath propagation characteristics at 60 GHz," *IEEE J. Sel. Areas Commun.*, vol. 14, pp. 441–448, Apr 1996.

[5] J. O. Nielsen and G. F. Pedersen, "Dual-polarized indoor propagation at 26 GHz," in *2016 IEEE 27th Annual International Symposium on Personal, Indoor, and Mobile Radio Communications (PIMRC)*, pp. 1–6, Sept 2016.

[6] J. Krogerus, J. Toivanen, C. Icheln, and P. Vainikainen, "User effect on total radiated power and 3-D radiation pattern of mobile handsets," *Antennas and Propagation, 2006. EuCAP 2006. First European Conference on*, pp. 1–6, Nov 2006.

[7] I. Syrytsin, S. Zhang, G. F. Pedersen, K. Zhao, T. Bolin, and Z. Ying, "Statistical investigation of the user effects on mobile terminal antennas for 5G applications," *IEEE Trans. Antennas Propag.*, 2017 (in press).

[8] I. Syrytsin, S. Zhang, and G. F. Pedersen, "Performance investigation of a mobile terminal phased array with user effects at 3.5 GHz for LTE advanced," *IEEE Antenna Wireless Propag. Lett.*, vol. 16, pp. 226–229, 2017.

[9] K. Zhao, J. Helander, D. Sjoberg, S. He, T. Bolin, and Z. Ying, "User body effect on phased array in user equipment for 5G mm wave communication system," *IEEE Antenna Wireless Propag. Lett.*, vol. 16, pp. 864–867, 2017.

[10] W. H. Zhang, W. J. Lu, and K. W. Tam, "A planar end-fire circularly polarized complementary antenna with beam in parallel with its plane," *IEEE Trans. Antennas Propag.*, vol. 64, pp. 1146–1152, Mar. 2016.

[11] M. You, W. J. Lu, B. Xue, L. Zhu, and H. B. Zhu, "A novel planar endfire circularly polarized antenna with wide axial-ratio beamwidth and wide impedance bandwidth," *IEEE Trans. Antennas Propag.*, vol. 64, pp. 4554–4559, Oct. 2016.

[12] C. Gabriel, S. Gabriel, and E. Corthout, "The dielectric properties of biological tissues: I. literature survey," *Phys. Med. Biol.*, vol. 41, pp. 2231–2249, 1996.

[13] J. Panero and M. Zelnik, *Human Dimension and Interior Space: A Source Book of Design Reference Standards*. Watson-Guptill, 1979.

[14] Health Examination Survey, The National Health and Nutrition Examination Surveys, and The Hispanic Health and Nutrition Examination Survey, *Anthropometric Reference Data for Children and Adults: United States, 2007–2010*. U.S. Government Printing Office, 2012.

[15] C. Telecommunications and I. A. (CTIA), "Test plan for wireless device over-the-air performance," *Revision Number 3.6.1*, November 2016.

[16] H. C. Burger and R. van Dongen, "Specific resistance of body tissues," *Phys. Med. Biol.*, vol. 5, no. 4, pp. 431–447, 1961.

[17] S. S. Zhekov, A. Tatomirescu, and G. F. Pedersen, "Antenna for ultrawideband channel sounding," *IEEE Antenna Wireless Propag. Lett.*, vol. 16, pp. 692–695, 2017.

0018-926X (c) 2018 IEEE. Personal use is permitted, but republication/redistribution requires IEEE permission. See http://www.ieee.org/publications_standards/publications/rights/index.html for more information.